

# Growth of Oxide Seed Layers on Ni and Other Technologically Interesting Metal Substrates: Issues Related to Formation and Control of Sulfur Superstructures for Texture Optimization

C. Cantoni, D. K. Christen, A. Goyal, L. Heatherly, F. A. List, G. W. Ownby, D. M. Zehner, H. M. Christen, and C. M. Rouleau

**Abstract**—The current carrying capabilities of RABiTS are connected to the crystalline quality of the seed buffer layer and the stability of the metal/seed layer interface. Our study shows that the epitaxial growth of commonly used seed layers on textured Ni is mediated by a sulfur superstructure present on the metal surface. Many structural defects generated during seed layer growth (secondary orientations, in-plane rotation, incomplete cube texture) can be related to the S surface concentration and superstructure coverage. More generally, our results indicate that the epitaxial deposition of several classes of oxides (fluorite, perovskite,  $\text{RE}_2\text{O}_3$ ) on several  $\{100\}\langle 100\rangle$  fcc metals depends, in addition to chemical stability and lattice match, on the existence and optimization of S superstructures on the metal surface. On these bases, we discuss issues related to the growth of different oxides on Ni, Ni-alloys, and Pd surfaces having different chemical and structural properties.

**Index Terms**—Buffer layers, coated conductors, epitaxial films, metal surface.

## I. INTRODUCTION

THE FABRICATION of rolling-assisted biaxially textured substrates (RABiTS) is based on the epitaxial deposition of an oxide film on a biaxially textured metal tape, typically Ni or Ni alloy. Recently, Oak Ridge National Laboratory and private companies like American Superconductor Corporation, 3M, and Microcoating Technology, in the US, have produced highly textured RABiTS tapes in meter lengths [1]. The scale up of this technology has involved transition from a typical stationary, short-sample buffer layer deposition to continuous, reel to reel texturing anneal and deposition processes. In the first stages of this effort it was found that uniformity and reproducibility of the seed buffer layer texture had not reached the level required for industrial production of RABiTS, and a better understanding of the oxide film nucleation on the metal surface was necessary.

We studied the surface of textured Ni, Ni alloy, and Pd substrates during annealing and oxide film growth using a pulsed laser deposition (PLD) system combined with *in situ* reflection high-energy electron diffraction (RHEED), Auger electron spectroscopy (AES), and x-ray diffraction (XRD). We found

that the structure and chemical composition of the textured Ni surface has a profound effect on the heteroepitaxial growth of entire classes of oxide seed layers.

In particular, our experiments revealed the existence of a sulfur superstructure on the textured Ni (or Ni alloy) surface that forms after surface segregation of sulfur contained as a common impurity in the metal bulk. During the high-temperature texturing anneal, S atoms diffuse to the surface of the tape and are arranged in a centered ( $2 \times 2$ ) superstructure. Depending on the initial S concentration and/or specific annealing conditions, the superstructure layer can exhibit different coverage.

Here we discuss the effect of such superstructure on the nucleation of several oxide layers on Ni, Ni alloys, and Pd surfaces. We also examine issues related to incomplete superstructure coverage, and describe a method for controlling the S surface concentration.

## II. SEED LAYERS ON $\{100\}\langle 100\rangle$ Ni

Among the various materials compatible with  $\text{YBa}_2\text{Cu}_3\text{O}_{7-\delta}$  (YBCO), the seed layers used in RABiTS (adopting various *in situ* and *ex situ* techniques) are oxides with perovskite structure ( $\text{SrTiO}_3$ ,  $\text{LaMnO}_3$ ), fluorite structure ( $\text{CeO}_2$ , and Y-stabilized  $\text{ZrO}_2$ ), pyrochlore structure ( $\text{La}_2\text{Zr}_2\text{O}_7$ ), and  $\text{RE}_2\text{O}_3$  structure ( $\text{Gd}_2\text{O}_3$ ,  $\text{Y}_2\text{O}_3$ ,  $\text{Eu}_2\text{O}_3$ ). The last two groups exhibit a crystal structure that differs from the fluorite by the presence of vacancies in the oxygen sublattice and cation order (in pyrochlores). The oxide seed layers investigated in this study are  $\text{CeO}_2$ , Y-stabilized  $\text{ZrO}_2$  (YSZ),  $\text{Gd}_2\text{O}_3$ ,  $\text{LaMnO}_3$  (LMO) and  $\text{SrTiO}_3$  (STO). For all these materials we found that deposition on the  $c$  ( $2 \times 2$ )-S template consistently produced highly textured (200) films, while deposition on a clean Ni surface always produced films with different orientation.

In order to produce clean Ni surfaces with the sulfur template, previously textured Ni tapes were heated to  $550^\circ\text{C}$  in high vacuum ( $P_b = 1 \times 10^{-8}$  Torr) for one hour to remove weakly bound species that had adsorbed on the surface after air exposure. This step was effective in removing any traces of hydrocarbons and oxygen on the sample surface. A stable S superstructure was at this point observed using RHEED and AES. An example of RHEED patterns is shown in Fig. 1 for two different orientations: with the incident electron beam parallel to the  $\langle 100\rangle$  (Fig. 1(a)) and to the  $\langle 100\rangle$  (Fig. 1(b)), respectively. The pattern in Fig. 1(a) shows two extra streaks (indicated by arrows) in addition to the

Manuscript received August 8, 2002. This paper was supported in part by the U.S. Department of Energy under Contract DE-AC05-00OR22725 and in part by the Oak Ridge National Laboratory, managed by UT-Battelle, LLC.

The authors are with the Oak Ridge National Laboratory, Oak Ridge, TN 37831 USA (e-mail: cantonic@ornl.gov).

Digital Object Identifier 10.1109/TASC.2003.811936

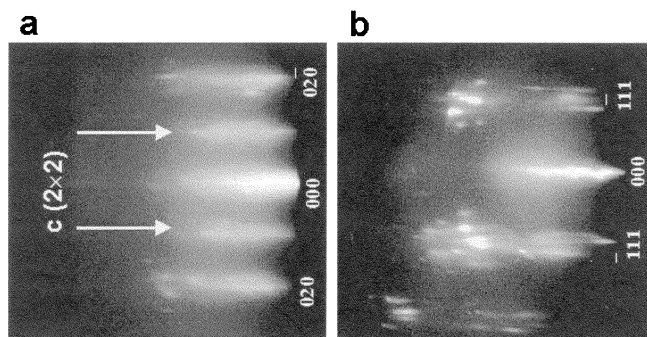


Fig. 1. RHEED patterns obtained from the  $\{100\}\langle 100 \rangle$  Ni surface after 1 hour anneal at  $500^\circ\text{C}$  with the incident electron beam along  $\langle 100 \rangle$ , (a); and along  $\langle 100 \rangle$ , (b). The Ni reflections are indexed and arrows indicate the superstructure streaks.

reflections observed for a clean Ni (001) surface pattern. The extra streaks are positioned halfway between the Ni streaks and are not observed in the  $\langle 110 \rangle$  pattern. This is consistent with the existence of a  $c(2 \times 2)$  S superstructure with S atoms occupying alternating four-fold hollow sites on the Ni surface lattice. AES spectra showed that the concentration of S on the surface was uniform across the sample and constant with temperature up to  $1000^\circ\text{C}$  in UHV conditions [2]. Ni surfaces free from sulfur were obtained by depositing a Ni film on the textured Ni tapes *in situ* by PLD. AES and RHEED analysis of laser deposited Ni overlayers indicated that these films did not contain any detectable amount of S. In these samples, segregation of sulfur to the surface and consequent formation of a  $c(2 \times 2)$  superstructure were observed only after the sulfur atoms had diffused through the entire Ni overlayer as a consequence of anneals at temperatures of  $750^\circ\text{C}$  or higher. However, RHEED observations indicated that the formation of the sulfur superstructure on the Ni films (500 Å–1000 Å thick) is a very slow process with a time constant of the order of 1 h or more. This justified the use of the samples with Ni overlayers as clean Ni surfaces in the seed layer deposition experiments. All seed layers were deposited by laser ablation of stoichiometric ceramic targets on the  $c(2 \times 2)/\{100\}\langle 100 \rangle$  Ni surface, and on the superstructure-free Ni overlayers that had been previously deposited *in situ*. The films were grown under the same conditions and with the same procedure for both types of samples, while monitoring the process with RHEED. The deposition temperature ranged between  $600^\circ\text{C}$  and  $800^\circ\text{C}$ .

In the case of YSZ and STO, after an initial  $\sim 100$ -Å-thick layer was deposited in vacuum ( $P_{\text{base}} \leq 5 \times 10^{-8}$  Torr), the  $\text{O}_2$  partial pressure was increased to  $1 \times 10^{-5}$  Torr and a final film was grown.  $\text{CeO}_2$  and  $\text{Gd}_2\text{O}_3$  seed layers were grown at a constant  $\text{H}_2\text{O}$  partial pressure of  $1\text{--}5 \times 10^{-5}$  Torr.  $\text{LaMnO}_3$  was grown using an  $\text{H}_2\text{O}$  partial pressure of 3–6 mTorr. Fig. 2 shows an XRD  $\phi$ -scan of the (111) peak for a  $\text{CeO}_2$  seed layer deposited on the  $c(2 \times 2)$ -S template. The first XRD peak appears at  $0^\circ$ , indicating that the  $\text{CeO}_2$  film had grown with a  $45^\circ$  in-plane rotation on the Ni substrate. This was also the case for YSZ and  $\text{Gd}_2\text{O}_3$  seed layers, while STO and LMO grew cube-on cube on the  $c(2 \times 2)$ -S template. Deposition of the same buffer layers on clean Ni surfaces gave rise to films with (111) orientation in the case of YSZ,  $\text{CeO}_2$  and  $\text{Gd}_2\text{O}_3$ ,  $\langle 001 \rangle$  seed// $\langle 001 \rangle$  Ni but multiple in-plane domains in the case of STO, and (110) orientation for LMO.

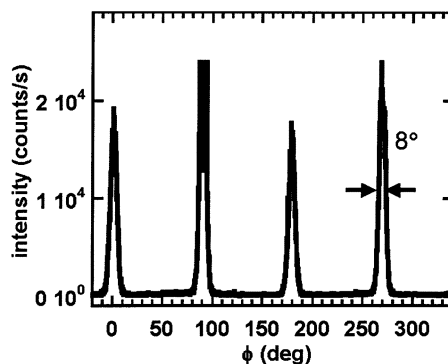


Fig. 2. XRD  $\phi$ -scan of the (111) peak for a  $\text{CeO}_2$  seed layer deposited on the  $c(2 \times 2)$  sulfur template chemisorbed on  $\{100\}\langle 100 \rangle$  Ni.

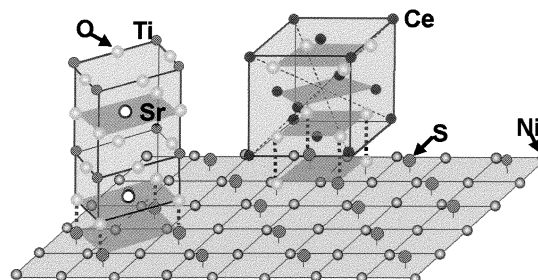


Fig. 3. Schematic model for the nucleation of  $\text{CeO}_2$  and STO on a (001) Ni surface with chemisorbed  $c(2 \times 2)$  sulfur superstructure. The dashed lines indicate correspondence between oxygen sites in (001) planes of the seed layer and sulfur sites on the Ni surface. The seed layer cations impinging on the Ni surface bond easily to the sulfur atoms present on the metal surface, promoting the (001) orientation of the growing film. In the STO case, there is a 1:1 correspondence between oxygen atoms in the SrO plane and sulfur atoms on the Ni surface. Therefore, it is plausible that Ti ions initially bond to the S surface atoms to form the first  $\text{TiO}_2$  plane of the STO structure. In the  $\text{CeO}_2$  case, two of four oxygen ions per unit cell match the sulfur atoms of the  $c(2 \times 2)$ . During nucleation of  $\text{CeO}_2$ , oxygen atoms may fill in the empty fourfold Ni hollows and the Ce cations subsequently bond to the template formed by S and O.

### III. QUANTIFICATION AND CONTROL OF THE S-SUPERSTRUCTURE

It is evident that the  $c(2 \times 2)$ -S superstructure plays a very important role in the nucleation of an oxide buffer layer on Ni. We propose that the effect of the S superstructure can be partially explained on the basis of structural and chemical considerations. The S layer behaves like a template that matches and mimics the arrangement of the oxygen atoms in (001) sub-lattice planes for all the seed layers considered in this study, as shown in Fig. 3. Sulfur belongs to the VI group and is chemically very similar to oxygen, often exhibiting the same electronic valence. The presence of such an ordered S template, thus, facilitates the bonding of the oxide cations in specific sites promoting the (001) epitaxial nucleation of the film.

In cases for which the bulk S content of particular batches of Ni was much lower than 30 p.p.m. by wt., the seed layer deposition process produced films with degraded texture or partial (111) orientation. In those cases, as recent Auger electron spectroscopy (AES) analyses revealed, S was depleted in the near-surface layer during a high temperature texturing anneal ( $\sim 1100^\circ\text{C}$ ). This may be the result of the formation and subsequent desorption of  $\text{SO}_2$  in the presence of a sufficient partial pressure of oxygen. Sulfur depletion impeded formation of a

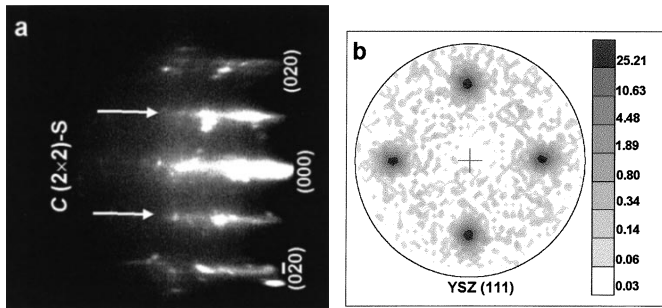


Fig. 4. RHEED pattern showing strong  $c(2 \times 2)$  reflections obtained after exposing a clean  $\{100\}\{100\}$  Ni surface to a few L of  $H_2S$  at  $800^\circ C$ . (a). Logarithmic (111) pole figure of a YSZ seed layer grown *in situ* on the  $c(2 \times 2)$ -S shown in (a). (b). For this sample the x-ray background signal was eliminated by subtracting a second pole figure obtained after changing the Bragg angle by 1 degree. The calculated percentage of cube texture for this film was 99.96%.

continuous  $c(2 \times 2)$  layer across the entire Ni surfaces, drastically modifying the oxide film nucleation.

The above-mentioned considerations illustrate a connection between the quality of the seed layer texture and the degree of coverage of the  $c(2 \times 2)$  superstructure on Ni. To investigate this, we conducted combined AES and RHEED experiments aimed at quantifying the coverage of the  $c(2 \times 2)$  structure on different Ni samples.

During AES experiments, depending on the material under test and the beam energy, Auger electrons escape and are detected from a layer 5 to  $10 \text{ \AA}$  deep below the surface. Therefore, the S concentration from AES can differ from the actual atomic concentration of the top monolayer of the surface [1], because of the uncertainty related to the measurement itself; and 2), because, after segregation, S could exhibit a concentration gradient in the layer tested by the Auger technique. We solved this ambiguity by comparing the AES results obtained on typical samples with those obtained on superstructure-free samples on which the  $c(2 \times 2)$  was intentionally grown through S adsorption. In these experiments, a clean Ni surface was first produced by depositing a Ni layer *in situ*. Subsequently, a small amount of  $H_2S$  with a partial pressure of  $5 \times 10^{-7} - 1 \times 10^{-6}$  Torr was introduced in the vacuum chamber at a substrate temperature of  $700-800^\circ C$  for few minutes and then pumped away. As shown by several other surface studies, the  $H_2S$  molecules dissociate at the Ni surface and S atoms chemisorb to form a superstructure with a coverage that saturates at 0.5 ML [1 ML  $\equiv$  (number of surface adsorbate atoms)/(number of surface substrate atoms)], corresponding to one complete atomic layer of the  $c(2 \times 2)$ -S [3]–[5]. Exposures to  $H_2S$  as low as a few L [1 L (langmuir)  $\equiv 10^{-6}$  Torr-s] produced very strong  $c(2 \times 2)$  reflections in the RHEED patterns as shown in Fig. 4(a). The sulfur superstructure was stable at  $800^\circ C$  after the  $H_2S$  was removed.  $CeO_2$  and YSZ seed layers deposited *in situ* after S adsorption were highly oriented with a percentage of cube texture very close to 100%, as indicated by the (111) pole figure of Fig. 4(b). Longer exposure of the Ni surface to  $H_2S$  ( $\geq 1800$  L) did not produce any degradation of the RHEED pattern that could be attributed to adsorption of surface S in excess of 0.5 ML, or formation of a Ni sulfide phase. After exposure to air at room temperature and consequent re-heating of the sample in vacuum, the as-grown superstructure was found to be stable and reproduced the same initial RHEED pattern. AES experiments performed *in situ* after S adsorption yielded a sulfur signal of about 25% at saturation. The same value was

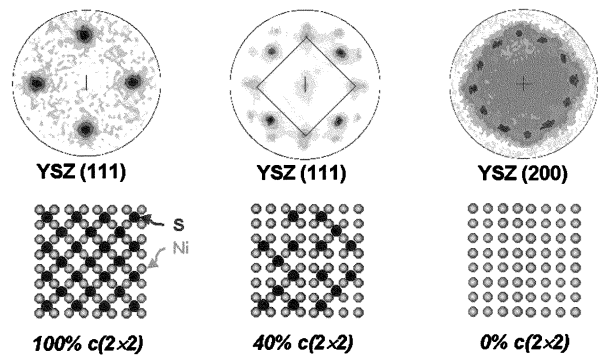


Fig. 5. Comparison between pole figures of 3 different STO films grown on  $\{100\}\{100\}$  Ni substrates having different sulfur coverage: 100% of a  $c(2 \times 2)$  layer (or  $\theta = 0.5$  ML) left; 40% middle; 0% right.

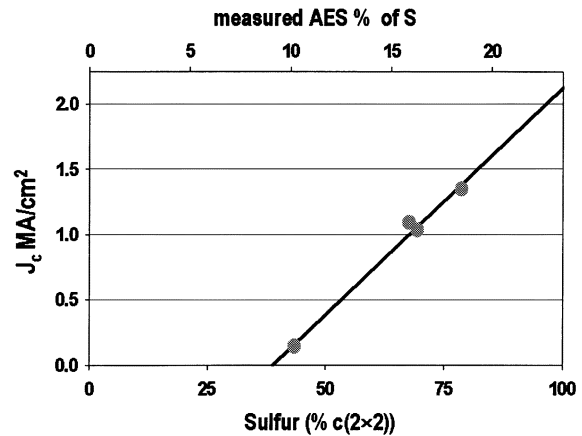


Fig. 6. Critical current density versus initial substrate S concentration for 4 YBCO/ $CeO_2$ /YSZ/ $CeO_2$ /Ni RABiTS samples.

obtained on samples where the  $c(2 \times 2)$ -S had formed as a consequence of segregation, and showed RHEED patterns identical to the ones acquired in the S adsorption experiments. From these observations we associated an AES value of  $\sim 25\%$  to a full layer of  $c(2 \times 2)$ -S on the Ni surface. Consequently, we were able to quantify the S surface content in cases in which the superstructure did not cover the entire Ni surface and the  $c(2 \times 2)$  reflections in the RHEED pattern were less intense than in fully covered samples.

Fig. 5 is a comparison of pole figures for a YSZ seed layer grown on three different types of Ni substrates. In the first case the substrate shows a complete S superstructure and the (111) logarithmic pole figure of the YSZ seed shows perfect cube texture. In the second case the substrate superstructure exhibit a partial coverage ( $\sim 40\%$ ) that translates to multiple orientation for the YSZ film. In the third case the surface of the substrate does not contain any S and the YSZ film shows only a (111) texture. In cases in which the substrate's S coverage was between 40 and 80% of a full  $c(2 \times 2)$  layer, we observed a cube texture with XRD peaks broader than those observed in seed layers grown on substrates with 100%  $c(2 \times 2)$ .

The improvement in the texture of the seed layer determined by the S superstructure corresponds to an enhancement in  $J_c$  of the YBCO film subsequently deposited on the completed (seed plus buffer layer) RABiTS substrate. This relation is illustrated in Fig. 6, which plots the critical current density of 4 YBCO/ $CeO_2$ /YSZ/ $CeO_2$ /Ni samples versus the S surface

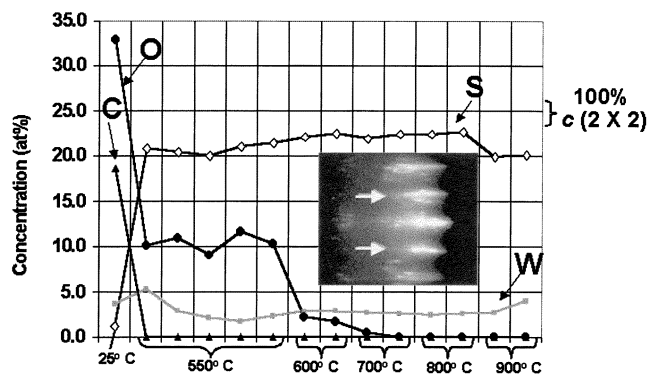


Fig. 7. AES data collected on a biaxially textured Ni-3%W alloy substrate after heating to different temperatures and holding for 10 or 60 minutes. The inset shows the RHEED pattern obtained after heating to 550°C.

content of the Ni substrate prior to seed layer deposition. In this experiment, the first sample was obtained by selecting a meter-long textured Ni tape showing only 40% of the S coverage corresponding to a full monolayer of  $c(2 \times 2)$ , and the other samples were exposed to  $H_2S$  in a subsequent anneal. In this case, the texturing anneal, sulfurization and seed layer ( $CeO_2$ ) deposition were carried out *in situ*, and continuously, in a reel-to-reel vacuum system equipped with an Auger spectrometer. The  $H_2S$  partial pressure was varied during the sulfurization treatment in such a way that different portions of the tape would show different S surface coverage at the end of the process. After deposition, 4 sections of the tape corresponding to 4 different S surface concentrations were cut and YBCO was deposited on them by PLD [6].

Sulfur adsorption experiments provide a method for quantifying the S coverage on the Ni surface after the texturing anneal. But, more importantly,  $H_2S$  exposure provides a rapid and efficient way to obtain a full coverage of the  $c(2 \times 2)$ -S on textured Ni, and, consequently, optimizes the seed layer texture without being restricted by the amount of S present in the bulk, which depend upon the less efficient segregation process.  $H_2S$  exposure has been successfully introduced in a continuous process for texturing and  $CeO_2$  coating of meter-long Ni tapes, yielding highly oriented and reproducible long lengths of RABiTS [6]. YBCO films deposited on short sections of these RABiTS tapes by PLD and *ex situ*  $BaF_2$  method have consistently shown critical current densities larger than  $1 \text{ MA/cm}^2$  [7].

#### IV. RESULTS OF SEED LAYER GROWTH ON Ni-3%W, Ni-13%Cr, AND Pd

Because of the magnetic properties of Ni, coated conductors fabricated using Ni tape show losses in AC electromagnetic fields, which pose a serious problem for certain applications [8]. Alloying Ni with small quantities of metals like W and Cr results in lower or practically zero magnetization at liquid  $N_2$  temperature (the latter is the case of the Ni-13%Cr alloy). In addition, Cr and W add strength to the tape, making handling of lengths easier.

Knowing the importance of the S superstructure for epitaxial seed layer growth on Ni, it is natural to wonder whether the superstructure plays the same role in textured Ni alloys. Fig. 7 shows Auger data and a RHEED pattern for a textured Ni-3%W substrate heated up to 900°C in high vacuum. It is evident that, just as for Ni, S surface segregation during texturing has resulted in a  $c(2 \times 2)$  superstructure with complete coverage. The

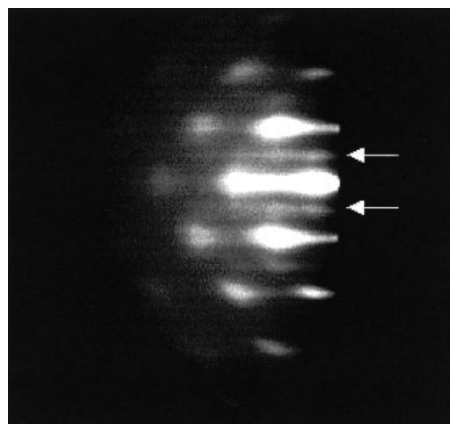


Fig. 8. RHEED pattern for a 100 nm-thick  $Gd_2O_3$  film on Ni-3%W.

oxygen and carbon signals in the Auger plot derive from air exposure after the texturing anneal, and these species desorb easily with mild heating. As expected from these observations, high quality buffer layers were deposited on such Ni-W surfaces.

Fig. 8 shows the RHEED pattern of a  $Gd_2O_3$  seed layer grown by PLD on a textured Ni-3%W substrate at a temperature of 600°C and a water pressure of  $1 \times 10^{-5}$  Torr. The figure indicates that the seed layer has grown epitaxially with (004) orientation. The weaker streaks marked by the arrows are superlattice reflections originated by the periodicity of the large cubic cell ( $a = 10.813$ ) of  $Gd_2O_3$  [9]. Fully textured  $CeO_2$ , YSZ and  $Y_2O_3$  seed layers have also been deposited on  $c(2 \times 2)$ -S/Ni-3%W, by PLD or other vapor deposition techniques, using the same growth conditions established for deposition on Ni. We would like to point out that, because of the higher reactivity of  $O_2$  with W, as compared to Ni, careful control of background oxygen is important during buffer layer deposition on Ni-W alloys. RHEED observations showed that while the Ni-3%W surface is stable in the presence of a water pressure in the range of  $10^{-5}$  Torr,  $H_2O$  pressures in the range of  $10^{-4}$  Torr or higher cause changes in the diffraction patterns that can be interpreted as oxide formation. The surface of pure Ni remained stable against oxidation at water pressures as high as tenths of mTorr.

The reactivity with oxygen is substantially higher for Ni-13%Cr substrates. In fact, attempts to deposit typical seed layers like  $CeO_2$  or  $Y_2O_3$  by several vapor deposition techniques on Ni-13%Cr have failed. A combination of RHEED and Auger measurements on these substrates has shown that C and O species are strongly bound to the Ni-Cr surface after air exposure, and high temperature anneals (700–750°C) in 200 mTorr of forming gas before deposition are necessary to clean the surface and expose the underlying S superstructure. Once cleaned, the Ni-13%Cr surfaces with the top  $c(2 \times 2)$ -S superstructure are stable in background oxygen pressures lower than  $1 \times 10^{-8}$  Torr. Above this value, oxidation of the substrate occurs rapidly disrupting seed layer growth. As mentioned above, the deposition conditions for most of the seed layers used for RABiTS involve a  $H_2O$  pressure of  $10^{-5}$  Torr or higher. Such a  $H_2O$  pressure in the deposition chamber gives rise to an equilibrium oxygen pressure in the range of  $10^{-7}$  Torr, as indicated by a quadrupole mass spectrometer, and therefore is sufficient to oxidize the Ni-13%Cr surface. The only successful attempt of oxide seed layer growth on the bare  $c(2 \times 2)$ /Ni-Cr surface by PLD was obtained using YSZ. Unlike other seed

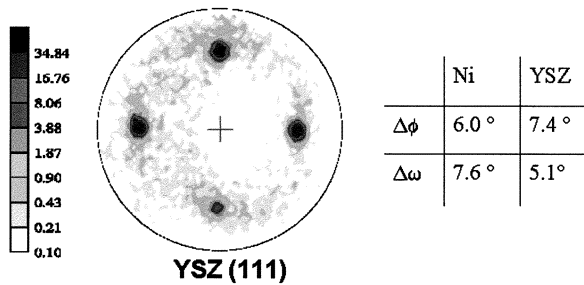


Fig. 9. Logarithmic (111) pole figure of a YSZ film deposited on  $c(2 \times 2)/\text{Ni}-13\% \text{Cr}$ .

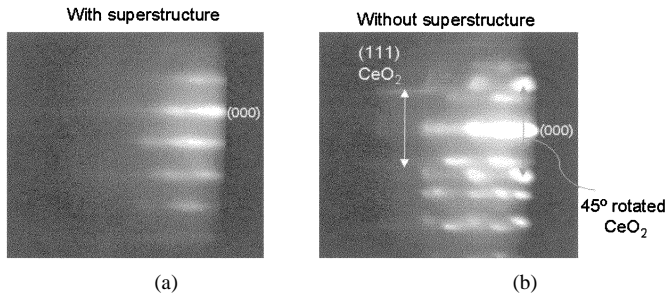


Fig. 10. RHEED patterns with e-beam parallel to the substrate  $\langle 100 \rangle$  for a  $\text{CeO}_2$  film nucleated on a Pd (001) surface with the S superstructure (a) and on a clean S-free Pd (001) surface.

layers, YSZ can be deposited from a ceramic target using an oxygen background pressure as low as  $10^{-10}$  Torr. Cube textured YSZ films were grown on Ni-13%Cr at a temperature of  $600^\circ\text{C}$  by ablation of a YSZ target in the base pressure of the vacuum chamber ( $0.5-1 \times 10^{-8}$  Torr, corresponding to an  $\text{O}_2$  partial pressure of  $0.5-1 \times 10^{-10}$  Torr). In addition to the (002) reflections, these films showed a small (111) component with no preferential in-plane orientation. The (111) component was not observed when the initial part of the YSZ deposition was conducted in a partial pressure of  $\text{H}_2\text{S}$  equal to  $2 \times 10^{-6}$  Torr. Fig. 9 shows the logarithmic YSZ (111) pole figure for a 170 nm thick film that was grown using  $\text{H}_2\text{S}$  for the initial layer of 70 nm in thickness. Although the background x-ray signal was subtracted in order to highlight possible secondary orientations, the pole figure shows only cube-texture reflections and the percentage of cube texture is 93%. Despite the chamber's low background oxygen pressure, activated oxygen species present in the ablation plume can probably lead to local formation of  $\text{CrO}_x$ , and consequently partial nucleation of YSZ with noncube orientation. The presence of  $\text{H}_2\text{S}$  during the first stage of film growth reduces the amount of oxygen in the plume by forming  $\text{SO}_2$  molecules. Consequently, the substrate oxidation rate decreases, allowing a well-textured YSZ film to be deposited. After the YSZ deposition, an 80-nm-thick  $\text{CeO}_2$  cap layer was grown *in situ* at  $660^\circ\text{C}$  in an oxygen partial pressure of  $5 \times 10^{-4}$  Torr. A 200-nm-thick YBCO film grown on this sample by PLD showed a  $J_c$  of  $0.44 \text{ MA/cm}^2$  at 77 K and in self magnetic field.

The structural model presented above for the S effect on seed layer epitaxy should in principle apply to any fcc metal surface that forms a  $c(2 \times 2)$  superstructure and has a good lattice match with the seed layers used in RABiTS fabrication. We found that Pd also forms a  $c(2 \times 2)$  superstructure, and, just like for Ni,  $\text{CeO}_2$  and STO seed layers can be grown epitaxially on such S template. The Pd (001) surfaces we considered were obtained by

depositing thick epitaxial Pd films on (001) STO single crystals by e-beam evaporation. The as-grown films were free of sulfur and the  $c(2 \times 2)$  superstructure was grown by *in situ*  $\text{H}_2\text{S}$  exposure, as done for Ni substrates. Fig. 10 shows a comparison of RHEED patterns acquired during the nucleation of a  $\text{CeO}_2$  film on a  $c(2 \times 2)$ -S/Pd surface and on a clean Pd surface respectively. In the latter case the RHEED pattern shows additional spots attributable to (111) oriented and  $45^\circ$  rotated crystal domains that are not observed when  $\text{CeO}_2$  is deposited on the S covered metal surface.

## V. CONCLUSION

In conclusion, the  $c(2 \times 2)$ -S superstructure is not only present on  $\{100\}\{100\}$  Ni but forms also on the surface of biaxially textured Ni-alloys such as Ni-3%W and Ni-13%Cr, and on Pd. In all cases, the  $c(2 \times 2)$ -S superstructure acts like a template that enables the epitaxial growth of oxide seed layers on the metal, and a complete coverage of this chemically stable layer is necessary to replicate the substrate texture in the buffer layer. Annealing the Ni, Ni-alloy, or Pd substrates at seed layer deposition temperature, in the presence of a small amount of  $\text{H}_2\text{S}$  is sufficient to produce a stable  $c(2 \times 2)$ -S with a coverage of 0.5ML. This simple step creates a complete S template independent of the coverage obtained through segregation. Implementing this step in a continuous RABiTS fabrication process allows the initial Ni/Ni-alloy texturing anneal to be carried out at conditions that yield the best texture (and often involve high temperatures and consequent S evaporation) without being limited by the S segregation process.

## ACKNOWLEDGMENT

The authors would like to thank P. Fleming (Oak Ridge National Laboratory, Solid State Division) for depositing the Pd films on STO substrates.

## REFERENCES

- [1] Results Presented at the 2002 DOE Peer Review on Superconductivity, Washington, DC, July 17-19, 2002.
- [2] C. Cantoni, D. K. Christen, R. Feenstra, D. P. Norton, A. Goyal, G. Ownby, and D. M. Zehener, "Quantification and control of the sulfur  $c(2 \times 2)$  superstructure on  $\{100\}\{100\}$  Ni for optimization of YSZ,  $\text{CeO}_2$  and  $\text{SrTiO}_3$  seed layers texture," *Appl Phys Lett*, vol. 79, pp. 3077-3079, Nov. 2001.
- [3] M. Perdureau and J. Oudar, "Structure, formation mechanism and stability of sulfur adsorption films on nickel," *Surf Sci.*, vol. 20, pp. 80-98, 1970.
- [4] S. Andersson, "Surface vibrations of oxygen and sulphur in the p (22) and c (22) structures on Ni(100)," *Surf Sci.*, vol. 79, pp. 385-393, August 1978.
- [5] C. A. Papageorgopoulos and M. Kamaratos, "Adsorption of Elemental S on Ni(100) Surfaces," *Surf Sci.*, vol. 352, pp. 364-368, May 1996.
- [6] M. M. Kowalewski, F. A. List, L. Heatherly, and D. M. Kroeger, "Continuous processing of coated conductors," in DOE Peer Review 2001, Washington, DC, [Online]. Available: <http://www.ornl.gov/HTSC/fy01peer.htm>.
- [7] R. Feenstra, T. B. Lindemer, J. D. Budai, and M. D. Galloway, "Effect of oxygen-pressure on the synthesis of  $\text{YBa}_2\text{Cu}_3\text{O}_{7-x}$  thin-films by postdeposition annealing," *J. Appl. Phys.*, vol. 69, no. 9, pp. 6569-6585, May 1991.
- [8] J. R. Thompson, A. Goyal, D. K. Christen, and D. M. Kroeger, "Ni-Cr textured substrates with reduced ferromagnetism for coated conductor applications," *Physica C*, vol. 370, no. 3, pp. 169-176, May 2002.
- [9] M. Paranthaman, D. F. Lee, A. Goyal, E. D. Specht, P. M. Martin, X. Cui, J. E. Mathis, R. Feenstra, D. K. Christen, and D. M. Kroeger, "Growth of biaxially textured  $\text{Re}_2\text{O}_3$  buffer layers on rolled-Ni substrates using reactive evaporation for HTS-coated conductors," *Supercond. Sci. Tech.*, vol. 12, no. 5, pp. 319-325, May 1999.